Photometric Stereo Reconstruction for Surface Analysis of Mucosal Tissue

Khemraj Emrith[1]

Greg Slabaugh[2]

Andrew Poullis[3]

Christopher Groves[3]

Melvyn Smith[1]

[1] University of the West of England
Bristol, UK

[2] City University London
London, UK

[3] St. George's Hospital
London, UK

Abstract

We introduce photometric stereo reconstruction for surface analysis of mucosal tissue. Photometric stereo captures images of a surface from a single camera, but illuminated from different light sources. From the set of images, a detailed surface reconstruction is estimated. We apply photometric stereo principles to mucosal tissue, which raises technical challenges due to its specular appearance. Following reconstruction of the surface, we apply surface analysis techniques based on differential geometry to detect regions that are locally spherical, suggestive of polyps. The research described in this paper is a first step towards a real-time clinical support system based on 3D reconstruction of human tissue for gastereoentrologic applications such as colonoscopy.

1 Introduction

Photometric stereo [8] is a computer vision technique that estimates a dense set of normal vectors of a surface photographed with a fixed camera and multiple light sources. Under the assumption of Lambertian reflectance, and a minimum of three known light source locations, surface normal vectors can be determined and then integrated to reconstruct a detailed surface topography in three dimensions.

In the context of medical imaging, photometric stereo (PS) has recently been explored in applications ranging from dermatology [3] to laparoscopy [7]. In this paper, we apply photometric stereo to mucosal tissue, which is tissue that is typically coated with fluid secreted by a mucous membrane. Although mucosal tissue appears in many places in the body, such as the nostrils and eyelids, we are mostly interested in applications to the gastereointestinal (GI) system, extending from the mouth to the anus. Endoscopic applications such as colonoscopy examine the colon and rectum for pathology such as polyps, whereas upper GI clinical applications inspect the esophagus, stomach, and duodenum for conditions such as Barrett's esophagus. Due to its capability for real-time 3D reconstruction of high resolution surface details, in addition to colour images, photometric stereo has much potential for detection, diagnosis, and monitoring of disease in the GI tract.

However, traditional endoscopic equipment is limited to 2D imaging, using standard video or multispectral techniques like narrow-band imaging. Recently there has been been growing interest in using two-camera endoscopy to create video feeds that can be viewed using 3D glasses. However, such systems do not actually acquire a 3D surface, rather two video streams that are presented to the endoscopist. We argue that additional useful information can be extracted from a 3D reconstruction of the surface using photometric stereo, and the recovered geometry can be analysed, ultimately as part of a clinical workflow.

In related work, Lv et al. [4] apply photometric stereo to reconstruct a phantom model of the human tongue to capture subtle surface anatomy such as the papillae. Perhaps most related to our work is that of [2, 5], which applies photometric stereo to both ex-vivo and in-vivo mucosal tissue. This work demonstrates the promise of photometric stereo to differentiate normal from abnormal tissue, even at diminutive sizes, but also highlights the challenge of imaging mucosal tissue, which produces specular highlights due to the fluid on the tissue.

In this paper we also apply photometric stereo to mucosal tissue. However, to our knowledge, this is the first paper to perform 3D shape analysis of mucosal tissue reconstructed using photometric stereo. We produce a proof-of-concept results demonstrating that photometric stereo is capable of capturing important geometric details that can be analysed using computational geometry. Inspired by the CT Colonography computer-aided detection literature, we apply simple differential geometric measures to the heightmap reconstructed from photometric stereo, and use them to define regions of interest in image, the first step in a computer-aided detection algorithm to identify suspicious pathology.

2 3D Reconstruction of Mucosal Tissue

In this section we investigate the effect of illuminating a porcine gut wall and capture images to recover the 3D surface topography of different patches of the GI tract. A key challenge is that mucosal surfaces are moist, producing specular reflections when photographed. We describe our vision-based approach and how it addresses this challenge.

Using a porcine gut model, photometric images were captured using a six-light source photometric stereo setup. Photometric stereo assumes diffuse reflectance from the illuminated surface. However, as shown in [2, 3], a Lambertian model can be used to approximate the reflectance characteristics of the mucosal surface by discarding patches with specular reflection. In this study we use a least squares approximation approach to estimate the surface in the presence of the highlights. Several areas of the porcine gastrointestinal tract were scanned. A Gig-E Basler Pilot camera with a resolution of 2448×2050 pixels was used to capture sets of photometric images from each area investigated. Figure 1 shows one set of photometric images, containing considerable specular highlights, captured from the colon part of the gastrointestinal tract. The highlights saturate the sensor on the imaging device, making the recovery of the surface at that those locations extremely challenging. If left unhandled, highlights result in discontinuities in the surface normals that are used estimate the 3D surface topography. The images are captured in sequence from six different illumination directions for the same observation point. The intensities and the illumination data is stacked, respectively, to form an intensity vector $\mathbf{I}(\mathbf{x},\mathbf{y}) = (I_1(x,y), I_2(x,y) \ldots I_6(x,y))$ and an illumination matrix $[\mathbf{L}] = (l_1, l_2, l_3)$. Assuming Lambertian reflectance, we write

$$\mathbf{I}(x,y) = p(x,y)\,(\mathbf{L}\cdot\mathbf{n})\,, \tag{1}$$

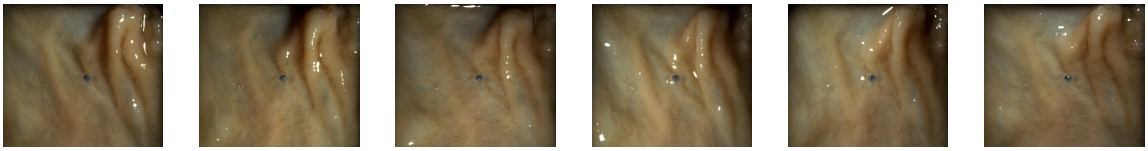

Figure 1: A sequence of six photometric images captured from a patch of duodenum of the porcine gut model used (zoom in for detail).

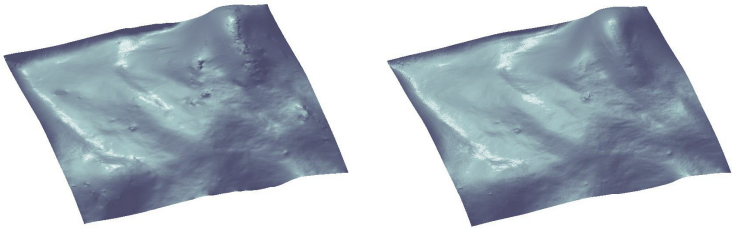

(a) (b)

Figure 2: Recovered 3D mucosal tissue under uniform illumination (a) without highlights elimination (b) with highlights elimination.

where $p(x,y)$ is the albedo and $\mathbf{n}$ is the surface normal. Assuming that matrix $\mathbf{L}$ is known, and is at least of rank 3 (i.e. three or more light sources are used), then the albedo and surface normal can be uniquely calculated using linear least-squares:

$$p = |\left(\mathbf{L}^T\mathbf{L}\right)^{-1}\cdot\mathbf{L}^T\cdot\mathbf{I}| \quad (2)$$

$$\mathbf{n} = \left(\left(\mathbf{L}^T\mathbf{L}\right)^{-1}\cdot\mathbf{L}^T\cdot\mathbf{I}\right)/p, \quad (3)$$

To eliminate discontinuities (highlights and shadows) that arise during capture, the stacked intensity values from the six different light sources are sorted at every pixel location and the smallest and largest values are eliminated as they are bound to represent either shadows (low intensity) or highlights (high intensity). The remaining intensity values at every pixel is then used to recover the 3D surface geometry of the patch of mucosal tissue being investigated. Figure 2(a) and (b) shows 3D surfaces from the sequence shown in Figure 1 rendered under uniform illumination. We observe that although the combined amount of highlights is not high, the recovered surface shown in Figure 2(a) contains distorted patches when the highlights are not eliminated as compared to the recovered 3D surface with highlights eliminated (see Figure 2(b)).

3 Surface Analysis

In this section we describe our approach to surface analysis, based on the recovered height field described in the previous section.

3.1 Differential geometry of height fields

A height field $f(x,y)$ describes a surface of the form $\mathbf{S} = (x,y,f(x,y))$, which provides a mapping from $\mathbb{R}^2 \rightarrow \mathbb{R}^3$.

In this paper we are interested in the differential geometric structure of the surface, which is characterised using the first and second fundamental forms [1], composed of coefficients of first order surface derivatives $E = \mathbf{S}_x \cdot \mathbf{S}_x$, $F = \mathbf{S}_x \cdot \mathbf{S}_y$, and $G = \mathbf{S}_y \cdot \mathbf{S}_y$, as well as second order surface derivatives $L = \mathbf{S}_{xx} \cdot \mathbf{n}$, $M = \mathbf{S}_{xy} \cdot \mathbf{n}$, $N = \mathbf{S}_{yy} \cdot \mathbf{n}$.

3.2 Surface measures

As the data is arranged on a square lattice in the form of an image, one can easily compute the above derivatives using finite differences. These derivatives are then used to compute the Mean (H), Gaussian (K), and principle curvatures (K_1 and K_2) for each point on the surface, leading the to shape index SI,

$$H = \frac{LN - M^2}{EG - F^2} \tag{4}$$

$$K = \frac{EN + GL - 2FM}{2(EG - F^2)} \tag{5}$$

$$K_1 = H + \sqrt{(H^2 - K)} \tag{6}$$

$$K_2 = H - \sqrt{(H^2 - K)} \tag{7}$$

$$SI = \frac{1}{2} - \frac{1}{\pi} \tan^{-1}\left(\frac{K_1 + K_2}{K_1 - K_2}\right) \tag{8}$$

The Shape Index (SI), which combines the two principal curvatures in a single measure, providing a local shape feature at each voxel. Every distinct shape, except for the plane, corresponds to a unique shape index. For example, a shape index value of 1.0 indicates a sphere-like shape (such as a polyps), while 0.75 indicates a cylinder-like shape (such as a haustral fold). Shape index can be computed at different scales by resampling the heightmap to a desired resolution.

4 Results

Our photometric stereo imaging system was used to produce five *ex-vivo* reconstructions of pig's gastereointestinal system, including the colon, duodenum (two images), oesophagus, and gasto-oesophageal junction, as shown in Figure 3, left three columns. A pig's gastereointestinal system is a good proxy for that of a human, with similar features such as haustral folds, and three longitudinal muscular bands (tenia). For this reason pig's colons are commonly used in training gastereoenterologists.

The heightmaps were analysed using the surface measures described in Section 3. Results are also shown in Figure 3, right two columns, for a course scale achieved by resampling the heightmap by a factor of 0.01. In this visualisation, the shape index values are clamped to the range [0.5, 1]. The values of the shape index that are highest correspond to places that are locally spherical, when both principle curvatures are large. These are good candidates for polyps, and indeed a segmentation of the shape index image may provide a useful way to establish candidate polypoidal regions, as is done in Computer-Aided Detection (CAD) systems designed for CT Colonography [9].

We perform a segmentation of the shape index using a hysteresis thresholding [6] technique, which relies on two thresholds (T_l, T_h) to define a region of interest. First, the shape index image is thresholded with the lower threshold, and connected component analysis is performed to identify connected regions with shape index above the lower threshold, T_l. These regions however may include anatomical regions that are not highly spherical. Each connected region is then checked based on T_h, and only the regions that contain at least one pixel above T_h are retained. In Figure 4 we show example segmentations of the shape index overlaid on top of the original images, for $[T_l, T_h] = [0.8, 0.98]$. The region of interest

does an excellent job of segmenting an artificial polyp, with a raised, hemispherical shape, created by a gastereoentrologist and shown in the second row of the figure. The current study shows that the 3D descriptors derived are highly suitable to detect polyps which are characterised by locally spherical regions in the GI tract. An extension to this work is to capture a large dataset of mucosal tissues, excised from patients due to potential presence of polyps (benign/malignant). Such a dataset would be used to generate 3D descriptors to train an automatic polyp detection system. Classification results and validation approaches will be provided in a follow-up study.

5 Conclusion

We presented a technique for photometric stereo reconstruction surface analysis of mucosal tissue. Whilst the dataset in this paper is limited to five reconstructions of a porcine model, it's clear that photometric stereo has much promise in endoscopy to capture important geometric features which can be analysed using computational geometry.

This paper is a first step towards a real-time photometric stereo endoscopy system that provides clinical support to the endoscopist through surface-based image enhancement, computer-aided detection, and diagnosis. A key issue to be resolved in realising this vision is miniaturisation of the hardware to achieve a form factor that is comparable to modern video endoscopic equipment. Related to this is the challenge of performing photometric stereo in a narrow, confined space, particularly when the camera view to the surface is non-fronto parallel. One these challenges are addressed, we plan to explore in-vivo human tests and build a computer-aided detection/diagnosis system to assist the gasteroenterologist.

References

[1] M. do Carmo. *Differential Geometry of Curves and Surfaces*. Prentice Hall, ISBN: 0132125897, 1976.

[2] Durr N. J., V. Parot, G. Traverso, W. P. Puricelli, B. J. Vakoc, N. S. Nishioka, and G. Gonzalez. Imaging colonic surface topography with photometric stereo endoscopy. In *Digestive Disease Week; American Society for Gastrointestinal Endoscopy*, 2014.

[3] Z. Liu, J. Sun, L. N. Smith, M. L. Smith, and R. Warr. Distribution quantification on dermoscopy images for computer-assisted diagnosis of cutaneous melanomas. *Medical and Biological Engineering and Computing*, 50:503–513, 2012.

[4] H. Lv, Y. Cai, and S. Guo. 3d reconstruction of tongue surface based on photometric stereo. In *Proc. International Conference on Signal Processing (ICSP)*, pages 1668–1671, 2012.

[5] V. Parot, D. Lim, G. Gonzalez, G. Traverso, Nishioka N. S., Vakoc B., and N. Durr. Photometric stereo endoscopy. *Journal of Biomedical Optics*, 18(7), 2013.

[6] M. Petrou and C. Petrou. *Image Processing: The Fundamentals*. Wiley, 2010.

[7] Collins T. and A. Bartoli. 3d reconstruction in laparoscopy with close-range photometric stereo. In *Medical Image Computing and Computer Aided Intervenions (MICCAI)*, pages 634–642, 2012.

[8] R. M. Woodham. Photometric method for determining surface orientation from multiple images. *Optical Engineering*, 19(1):139–144, 1980.

[9] H. Yoshida and J. Nappi. Three-dimensional computer-aided diagnosis scheme for detection of colonic polyps. *Transactions on Medical Imaging*, 20(12):1261–1274, 2001.

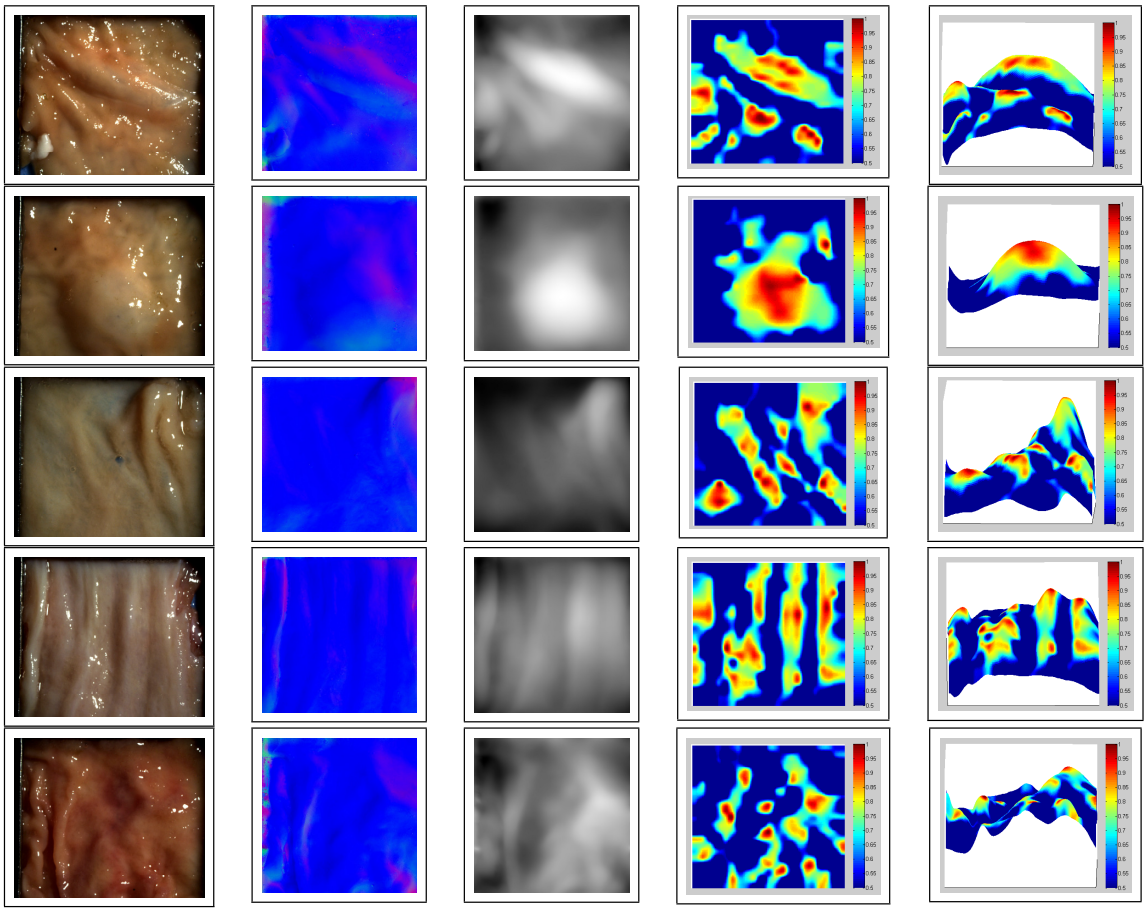

Figure 3: Data captured using the photometric stereo system. From left to right: one of the six images (left column), reconstructed normal map (second column), and reconstructed height map (middle column). From top to bottom: colon, duodenum, duodenum, oesophagus, gasto-oesophageall junction. The shape index is plotted on the surface, shown in a top view (fourth column) and side view (right column).

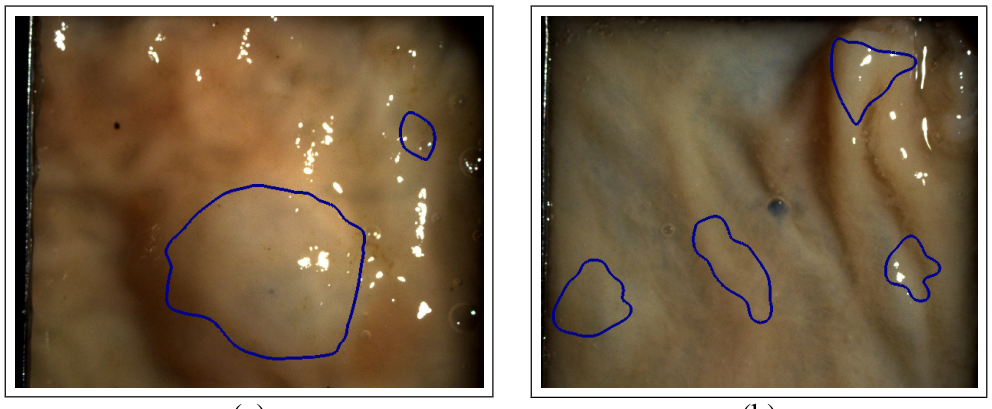

(a) (b)

Figure 4: Example segmentations using a hysteresis thresholding technique applied to the shape index image. These provide regions of interest that are locally spherical in the image.